Acta Cryst E CRYSTALLOGRAPHIC COMMUNICATIONS

ISSN 2056-9890

Crystal structure, Hirshfeld surface and crystal void analysis, intermolecular interaction energies, DFT calculations and energy frameworks of 2*H*-benzo[*b*][1,4]thiazin-3(4*H*)-one 1,1-dioxide

Ezaddine Irrou,[a]* Younesse Ait Elmachkouri,[a] Ahmed Mazzah,[b] Tuncer Hökelek,[c] Amal Haoudi,[d] Joel T. Mague,[e] Mohamed Labd Taha[a] and Nada Kheira Sebbar[a,f]

[a]Laboratory of Organic and Physical Chemistry, Applied Bioorganic Chemistry Team, Faculty of Sciences, Ibn Zohr University, Agadir, Morocco, [b]University of Lille, CNRS, UAR 3290, MSAP, Miniaturization for Synthesis, Analysis and Proteomics, F-59000 Lille, France, [c]Department of Physics, Hacettepe University, 06800 Beytepe, Ankara, Türkiye, [d]Laboratory of Applied Organic Chemistry, Faculty of Science and Technology, University of Sidi Mohamed Ben Abdellah BP 2202, Fez, Morocco, [e]Department of Chemistry, Tulane University, New Orleans, LA 70118, USA, and [f]Laboratory of Heterocyclic Organic Chemistry, Medicines Science Research Center, Pharmacochemistry Competence Center, Mohammed V University in Rabat, Faculté des Sciences, Av. Ibn Battouta, BP 1014, Rabat, Morocco. *Correspondence e-mail: ezaddine.irrou@edu.uiz.ac.ma

Received 13 September 2023
Accepted 3 October 2023

Edited by M. Weil, Vienna University of Technology, Austria

This article is part of a collection of articles to commemorate the founding of the African Crystallographic Association and the 75th anniversary of the IUCr.

Keywords: Crystal structure; hydrogen bond; C—H···π(ring) interaction; π-stacking; sulfone; crystal structure.

CCDC reference: 2298958

Supporting information: this article has supporting information at journals.iucr.org/e

In the title molecule, $C_8H_7NO_3S$, the nitrogen atom has a planar environment, and the thiazine ring exhibits a screw-boat conformation. In the crystal, corrugated layers of molecules parallel to the *ab* plane are formed by N—H···O and C—H···O hydrogen bonds together with C—H···π(ring) and S=O···π(ring) interactions. The layers are connected by additional C—H···O hydrogen bonds and π-stacking interactions. Hirshfeld surface analysis indicates that the most important contributions for the crystal packing are from H···O/O···H (49.4%), H···H (23.0%) and H···C/C···H (14.1%) interactions. The volume of the crystal voids and the percentage of free space were calculated as 75.4 Å^3 and 9.3%. Density functional theory (DFT) computations revealed N—H···O and C—H···O hydrogen-bonding energies of 43.3, 34.7 and 34.4 kJ mol^{-1}, respectively. Evaluation of the electrostatic, dispersion and total energy frameworks indicate that the stabilization is dominated *via* the electrostatic energy contribution. Moreover, the DFT-optimized structure at the B3LYP/ 6–311 G(d,p) level is compared with the experimentally determined molecular structure in the solid state. The HOMO–LUMO behaviour was elucidated to determine the energy gap.

1. Chemical context

Numerous heterocyclic compounds containing sulfur and nitrogen have been extensively studied because of their various biological applications (Gowda *et al.*, 2011; Sebbar *et al.*, 2020*a*; Fringuelli *et al.*, 2005). In this respect, 1,4-benzothiazine derivatives possess various pharmacological properties and have therapeutic applications such as antifungal (Kamila *et al.*, 2006), anti-inflammatory (Gowda *et al.*, 2011), antagonistic (Corelli *et al.*, 1997), anti-tumour (Abbas & Farghaly, 2010), antioxidant (Bakavoli *et al.*, 2008), antipyretic (Warren & Knaus, 1987), antihypertensive (Fringuelli *et al.*, 2005) or antibacterial effects (Sebbar *et al.*, 2016, 2020*a*).

Continuing our research on the development of new 1,4-benzothiazine derivatives with potential pharmacological applications, we carried out the oxidation of 3,4-dihydro-2*H*-1,4-benzothiazin-3-one by potassium permanganate in order to obtain 2*H*-benzo[*b*][1,4]thiazin-3(4*H*)-one 1,1-dioxide (I) with good yield. We report herein the molecular and crystal structure of this compound, as well as Hirshfeld surface

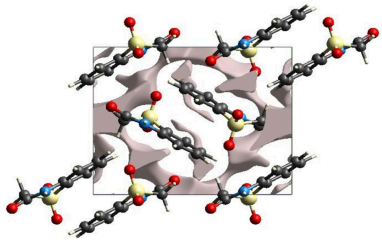

OPEN ACCESS
Published under a CC BY 4.0 licence

analysis and DFT-computational studies carried out at the B3LYP/6–31 G(d,p) and B3LYP/6–311 G(d,p) levels.

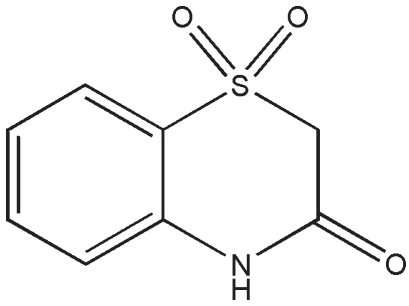

2. Structural commentary

A puckering analysis (Cremer & Pople, 1975) of the thiazine ring (C1, C6, N1, C7, C8, S1) gave the parameters Q = 0.5138 (6) Å, θ = 60.49 (7)° and φ = 326.72 (8)°. The distorted screw-boat conformation places O2 in an axial position and O3 in a pseudo-equatorial position (Fig. 1). The angles about N1 sum up to 360° within experimental error, indicating involvement of the lone pair in the C–N bond. This is reflected in the N1—C7 and N1—C6 distances of 1.3661 (9) and 1.4043 (9) Å, respectively.

3. Supramolecular features

In the crystal, N1—H1···O3 hydrogen bonds (Table 1) form chains of molecules extending parallel to the *a* axis. These chains are connected into corrugated layers parallel to the *ab* plane by C8—H8*B*···O2 hydrogen bonds together with C8—H8*A*···*Cg*2 and S1═O2···*Cg*2^{i} interactions [O2···*Cg*2 = 3.6233 (7) Å, S1···*Cg*2 = 4.1655 (5) Å, S1═O2···*Cg*2^{i} = 101.77 (3)°; symmetry code: (i) $-x+\frac{1}{2}, y+\frac{1}{2}, -z+\frac{3}{2}$; Fig. 2]. The layers are connected by C5—H5···O1 hydrogen bonds (Table 1) and slipped π–π stacking interactions between inversion-related C1–C6 rings [*Cg*2···*Cg*2($1-x, 1-y, 1-z$) = 3.7353 (5) Å, slippage = 1.55 Å] into a tri-periodic network structure (Fig. 3).

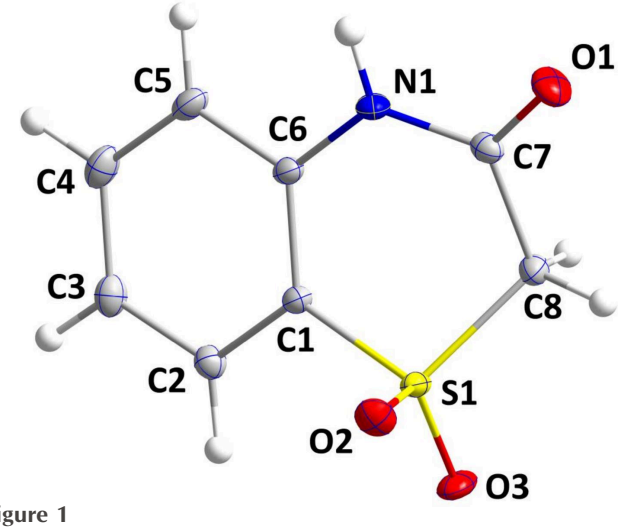

Figure 1
The title molecule with atom labelling and displacement ellipsoids drawn at the 50% probability level.

Table 1
Hydrogen-bond geometry (Å, °).

*Cg*2 is the centroid of the C1–C6 benzene ring.

D—H···*A*	*D*—H	H···*A*	*D*···*A*	*D*—H···*A*
N1—H1···O3^{i}	0.89 (1)	2.08 (1)	2.9472 (8)	165 (1)
C5—H5···O1^{ii}	0.95	2.58	3.2330 (9)	126
C8—H8*A*···*Cg*2^{iii}	0.99	2.93	3.7933 (8)	146
C8—H8*B*···O2^{iv}	0.99	2.39	3.2126 (9)	140

Symmetry codes: (i) $x+1, y, z$; (ii) $-x+\frac{3}{2}, y-\frac{1}{2}, -z+\frac{3}{2}$; (iii) $-x+\frac{1}{2}, y+\frac{1}{2}, -z+\frac{3}{2}$; (iv) $-x+\frac{1}{2}, y-\frac{1}{2}, -z+\frac{3}{2}$.

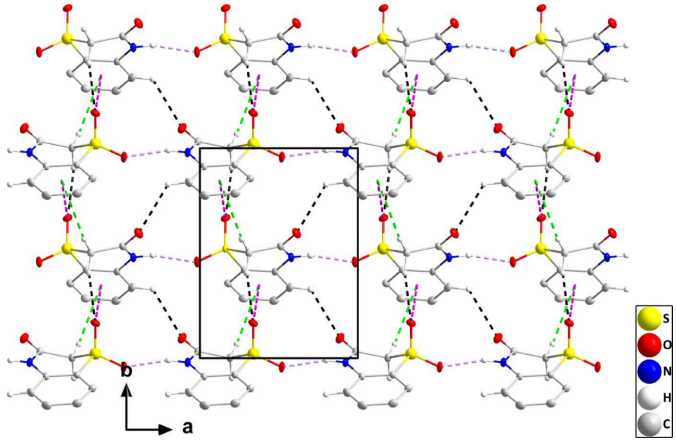

Figure 2
The crystal structure of (I) viewed along the *c* axis with N—H···O and C—H···O hydrogen bonds depicted, respectively, by violet and black dashed lines. C—H···π(ring) and C═O···π(ring) interactions are depicted, respectively, by green and dark-pink dashed lines and non-interacting hydrogen atoms are omitted for clarity.

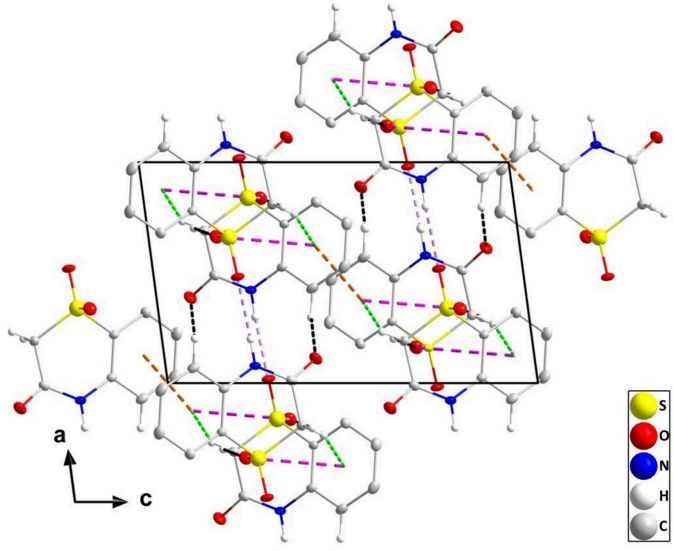

Figure 3
The crystal structure of (I) viewed along the *b* axis with N—H···O and C—H···O hydrogen bonds depicted, respectively, by violet and black dashed lines. C—H···π(ring), C═O···π(ring) and slipped π-stacking interactions are depicted, respectively, by green, dark-pink and orange dashed lines. Non-interacting hydrogen atoms are omitted for clarity.

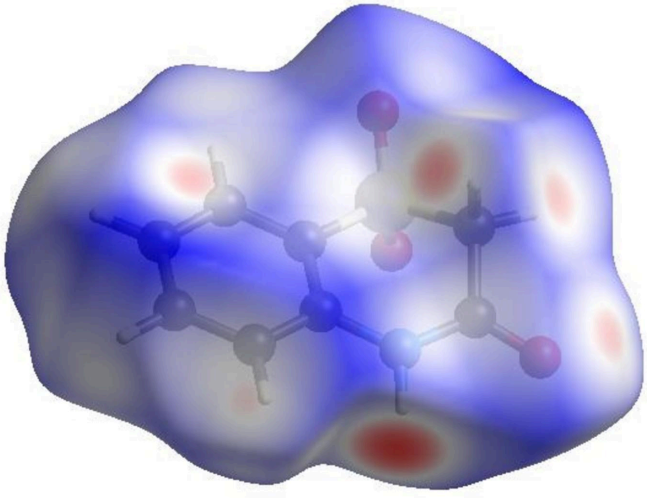

Figure 4
View of the three-dimensional Hirshfeld surface of (I) plotted over d_{norm}.

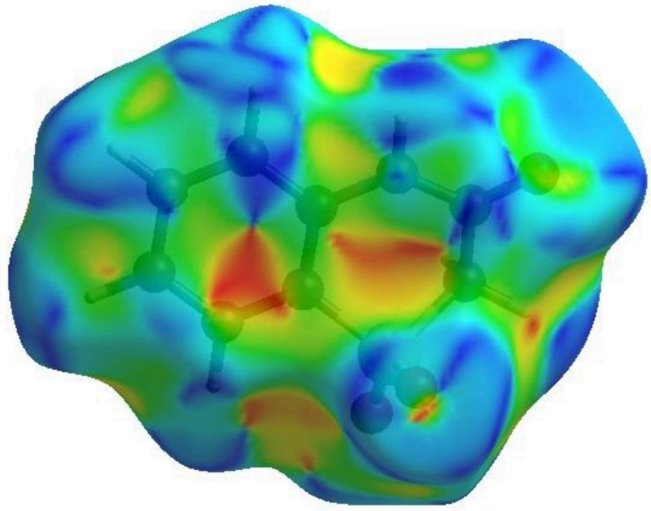

Figure 6
Hirshfeld surface of (I) plotted over shape-index.

4. Hirshfeld surface analysis

To visualize the intermolecular interactions in the crystal of (I), a Hirshfeld surface (HS) analysis (Hirshfeld, 1977) was carried out with *Crystal Explorer* (Spackman *et al.*, 2021). In the HS plotted over d_{norm} in the range −0.4976 to 1.2253 a.u. (Fig. 4), the white surface indicates contacts with distances equal to the sum of van der Waals radii and the red and blue colours indicate distances shorter (in close contact) or longer (distant contact) than the van der Waals radii, respectively (Venkatesan *et al.*, 2016). The bright-red spots indicate their roles as the respective donors and/or acceptors; they also appear as blue and red regions corresponding to positive and negative potentials on the HS mapped over electrostatic potential (Spackman *et al.*, 2008; Jayatilaka *et al.*, 2005) in the range −0.05 to 0.05 a.u., as shown in Fig. 5. The blue regions indicate positive electrostatic potential (hydrogen-bond donors), while the red regions indicate negative electrostatic potential (hydrogen-bond acceptors). The shape-index of the HS is a tool to visualize the π–π stacking by the presence of adjacent red and blue triangles. Fig. 6 clearly suggests that there are π–π interactions in (I). The overall two-dimensional fingerprint plot, Fig. 7*a*, and those delineated into H···O/O···H, H···H, H···C/C···H, C···O/O···C,C···C, H···N/

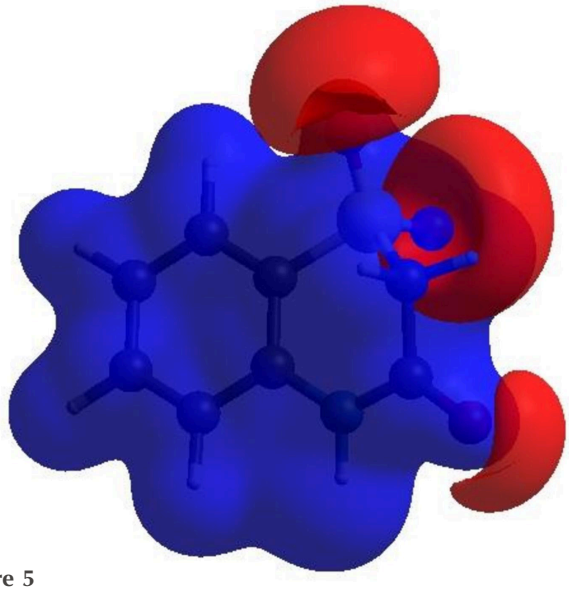

Figure 5
View of the three-dimensional Hirshfeld surface of (I) plotted over electrostatic potential energy using the STO-3 G basis set at the Hartree–Fock level of theory.

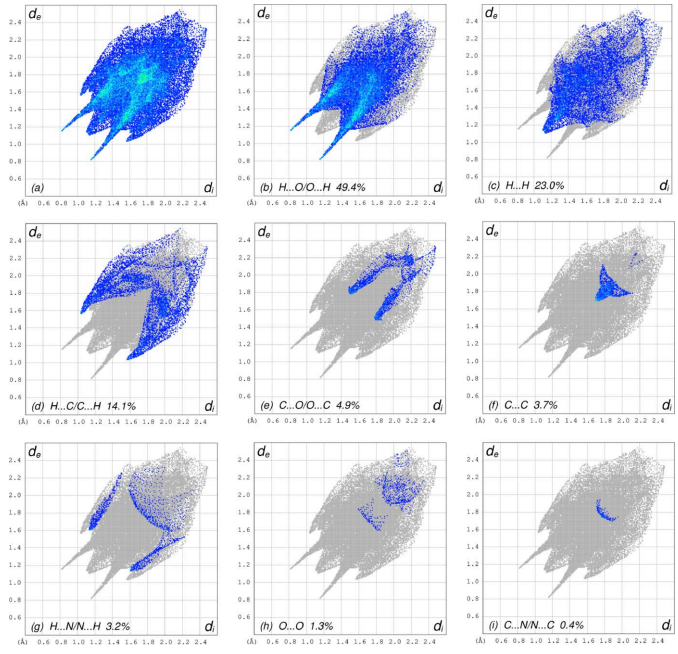

Figure 7
The full two-dimensional fingerprint plots for the title compound, showing (*a*) all interactions, (*b*) H···O/O···H, (*c*) H···H, (*d*) H···C/C···H, (*e*) O···C/C···O, (*f*) C···C, (*g*) H···N/N···H, (*h*) O···O and (*i*) C···N/N···C interactions. The d_i and d_e values are the closest internal and external distances (in Å) from given points on the Hirshfeld surface contacts.

N···H, O···O and C···N/N···C contacts (McKinnon *et al.*, 2007) are illustrated in Fig. 7*b–i*, respectively, together with their relative contributions to the Hirshfeld surface. The most important interaction is H···O/O···H, contributing 49.4% to the overall crystal packing, which is reflected in Fig. 7*b*, where the symmetric pair of spikes is observed with the tips at $d_e + d_i$ = 1.98 Å. The H···H contacts contribute 23.0% to the overall crystal packing, which is reflected in Fig. 7*c* as widely scattered points of high density due to the large hydrogen content of the molecule with the tip at $d_e = d_i$ = 1.13 Å. In the presence of C—H···π interactions, the pair of characteristic wings in the fingerprint plot delineated into H···C/C···H contacts, Fig. 7*d*, make a 14.1% contribution to the HS and viewed with the tips at $d_e + d_i$ = 2.59 Å. The wing pair of C···O/O···C contacts (Fig. 7*e*) with 4.9% contribution to the HS is viewed at $d_e + d_i$ = 3.30 Å. The C···C contacts (Fig. 7*f*) appearing as a bullet-shaped distribution of points make a contribution of 3.7% to the HS with the tip at $d_e = d_i$ = 1.70 Å. The spikes of H···N/N···H contacts (Fig. 7*g*) with 3.2% contribution to the HS are viewed at $d_e + d_i$ = 2.75 Å. Finally, the O···O (Fig. 7*h*) and C···N/N···C (Fig. 7*i*) contacts contribute 1.3% and 0.4%, respectively, to the HS. The Hirshfeld surface representations with the function d_{norm} plotted onto the surface are shown for the H···O/O···H, H···H and H···C/C···H interactions in Fig. 8*a–c*, respectively. The Hirshfeld surface analysis confirms the importance of H-atom contacts in establishing the packing. The large number of H···O/O···H, H···H and H···C/C···H interactions suggest that van der Waals interactions play the major role in the crystal packing (Hathwar *et al.*, 2015).

The strength of the crystal packing is important for determining the response to an applied mechanical force. If the crystal packing results in significant voids, then the molecules

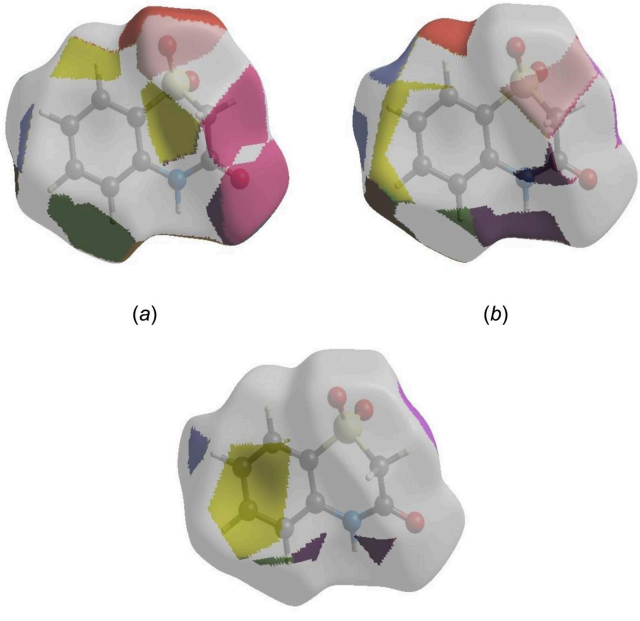

Figure 8
Hirshfeld surface representations of (I) with the function d_{norm} plotted onto the surface for (*a*) H···O/O···H, (*b*) H···H and (*c*) H···C/C···H interactions.

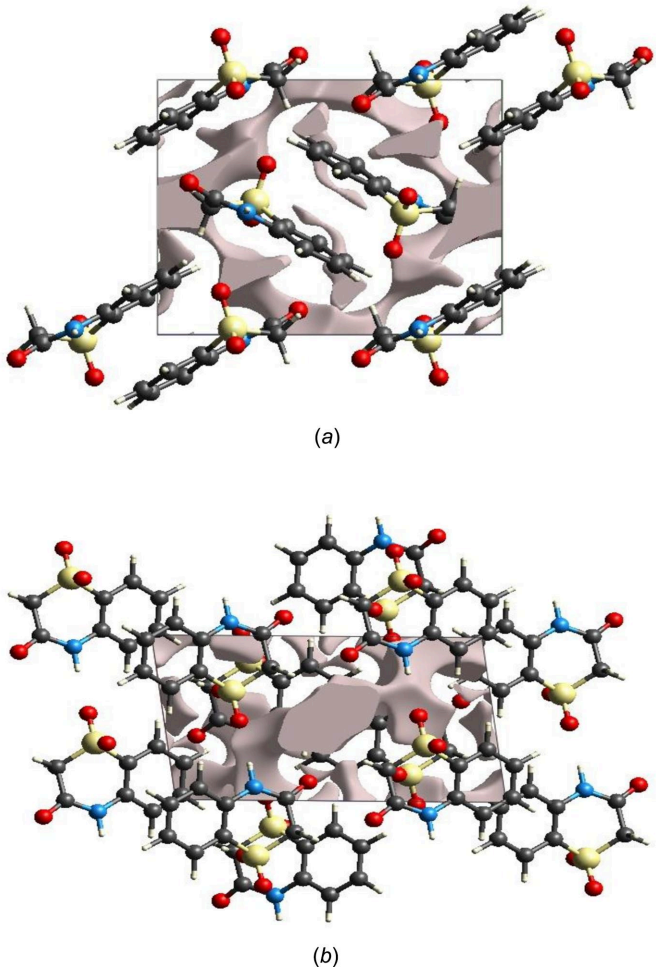

Figure 9
Graphical views of voids in the crystal packing of (I), (*a*) along the *a* axis and (*b*) along the *b* axis.

are not tightly packed and a small amount of applied external mechanical force may easily break the crystal. To check the mechanical stability of the crystal, a void analysis was performed by adding up the electron densities of the spherically symmetric atoms contained in the asymmetric unit (Turner *et al.*, 2011). The void surface is defined as an isosurface of the procrystal electron density and is calculated for the whole unit cell where the void surface meets the boundary of the unit cell and capping faces are generated to create an enclosed volume. The volume of the crystal voids (Fig. 9*a*,*b*) and the percentage of free space in the unit cell are calculated as 75.4 Å^3 and 9.3%, respectively. Thus, the crystal packing appears compact and the mechanical stability should be substantial.

5. Interaction energy calculations and energy frameworks

The intermolecular interaction energies were calculated using the CEB3LYP/631G(d,p) energy model available in *CrystalExplorer* (Spackman *et al.*, 2021), where a cluster of molecules is generated by applying crystallographic symmetry operations

with respect to a selected central molecule within the radius of 3.8 Å by default (Turner *et al.*, 2014). The total intermolecular energy (E_{tot}) is the sum of electrostatic (E_{ele}), polarization (E_{pol}), dispersion (E_{dis}) and exchange-repulsion (E_{rep}) energies (Turner *et al.*, 2015) with scale factors of 1.057, 0.740, 0.871 and 0.618, respectively (Mackenzie *et al.*, 2017). Hydrogen-bonding interaction energies (in kJ mol^{-1}) were calculated to be [−18.5 (E_{ele}), −5.2 (E_{pol}), −41.4 (E_{dis}), 26.2 (E_{rep}) and −43.3 (E_{tot})] for N1—H1···O3, [−22.4 (E_{ele}), −4.8 (E_{pol}), −28.3 (E_{dis}), 27.9 (E_{rep}) and −34.7 (E_{tot})] for C8—H8*B*···O2 and [−20.6 (E_{ele}), −5.8 (E_{pol}), −24.6 (E_{dis}), 21.2 (E_{rep}) and −34.4 (E_{tot})] for C5—H5···O1.

Energy frameworks combine the calculation of intermolecular interaction energies with a graphical representation of their magnitude (Turner *et al.*, 2015). Energies between molecular pairs are represented as cylinders joining the centroids of pairs of molecules with the cylinder radius proportional to the relative strength of the corresponding interaction energy. Energy frameworks were constructed for E_{ele} (shown in Fig. 10), E_{dis} and E_{tot}. The evaluation of the electrostatic, dispersion and total energy frameworks indicate that the stabilization is dominated *via* the electrostatic energy contribution in the crystal structure of (I).

6. DFT calculations

The optimized structure of (I) was computed in the gas phase using density functional theory (DFT) with the standard B3LYP functional and 6–311 G(d,p) basis-set calculations (Becke, 1993), employing the *GAUSSIAN 09* software (Frisch *et al.*, 2009). The theoretical and experimental results exhibit a good agreement, as summarized in Table 2.

The highest-occupied molecular orbital (HOMO), functioning as an electron donor, and the lowest-unoccupied molecular orbital (LUMO), acting as an electron acceptor, serve as vital parameters in quantum chemistry. A small energy gap signifies high molecular polarizability and enhanced chemical reactivity. The DFT calculations provided crucial insights into the reactivity and site selectivity of the molecular framework. Parameters such as E_{HOMO} and E_{LUMO}, electronegativity (χ), hardness (η), dipole moment (μ), electrophilicity (ω) and softness (σ) are compiled in Table 3. Both η and σ are essential for assessing reactivity and stability. The electron transition from HOMO to LUMO energy levels is depicted in Fig. 11. Notably, both HOMO and LUMO are

Table 2
Comparison of the selected (X-ray and DFT) geometric data (Å, °).

Bonds/angles	X-ray	B3LYP/6–311G(d,p)
S1—O2	1.4450 (6)	1.50996
S1—O3	1.4464 (6)	1.59088
S1—C1	1.7478 (6)	1.78874
S1—C8	1.7649 (7)	1.80529
O1—C7	1.2203 (8)	1.21656
N1—C7	1.3661 (9)	1.37417
N1—C6	1.4043 (9)	1.39867
O2—S1—O3	117.64 (4)	118.09813
O2—S1—C1	109.21 (3)	109.40063
O3—S1—C1	109.56 (3)	109.84640
O2—S1—C8	108.59 (3)	109.10007
O3—S1—C8	109.59 (3)	109.62080
C1—S1—C8	100.95 (3)	99.96775
C7—N1—C6	127.24 (6)	127.88849
C7—N1—H1	116.1 (10)	115.98354

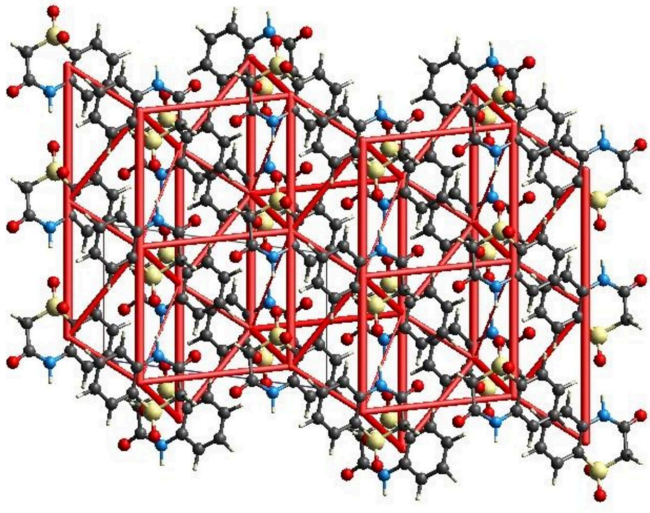

Figure 10
The energy framework for the electrostatic energy, viewed down the *b* axis for a cluster of molecules, where the *a* axis is vertical and the *c* axis is horizontal. The cylindrical radius is proportional to the relative strength of the corresponding energy and adjusted to the scale factor of 80 with a cut-off value of 5 kJ mol^{-1} within 2 × 2 × 2 unit cells.

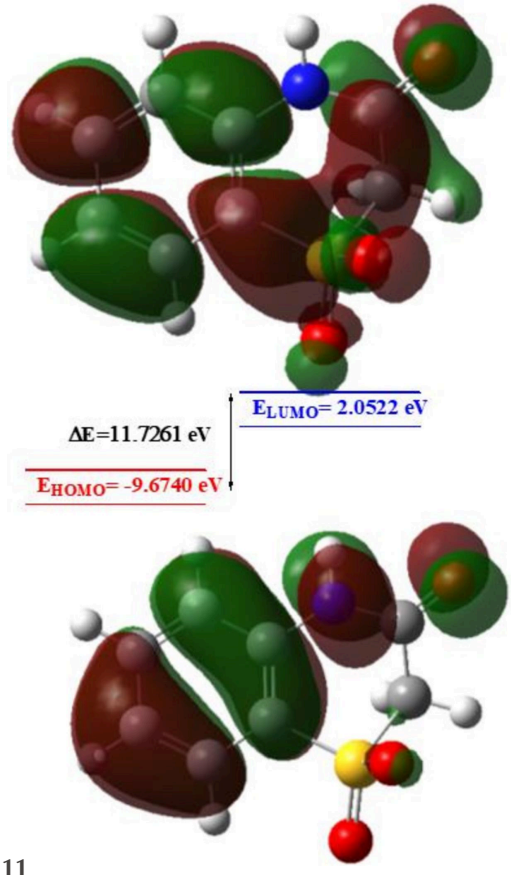

Figure 11
The energy band gap of (I).

Table 3
Calculated energies.

Molecular Energy (a.u.) (eV)	Compound (I)
Total Energy, *TE* (eV)	−26615,8936
E_{HOMO} (eV)	−9.6740
E_{LUMO} (eV)	2.0522
Gap, ΔE (eV)	11.7261
Dipole moment, μ (Debye)	7.583751
Ionization potential, *I* (eV)	9.6740
Electron affinity, *A*	2.0522
Electronegativity, χ	−3.8109
Hardness, η	−5.8631
Electrophilicity index, ω	−1.2385
Softness σ,	−0.1706
Fraction of electron transferred, ΔN	−0.9219

localized within the plane spanning the entire 2H-benzo[*b*]-[1,4]thiazin-3(4*H*)-one 1,1-dioxide ring. The energy band gap [$\Delta E = E_{LUMO} - E_{HOMO}$] for the molecule is 11.7261 eV, and the energies of the frontier molecular orbitals, E_{HOMO} and E_{LUMO}, are −9.6740 eV and 2.0522 eV, respectively.

7. Database survey

A search in the Cambridge Structural Database (CSD, updated March 2023; Groom *et al.*, 2016) for compounds containing the fragment **II** (*R*1 = Ph or 2-ClC_6H_4, *R*2 = C; Fig. 12), gave 14 hits. With *R*1 = Ph, and with *R*2 = $CH_2COOCH_2CH_3$ (**IIa**; Sebbar *et al.*, 2020*b*), CH_2COOH (**IIb**; Sebbar *et al.*, 2016), $CH_2C{\equiv}CH$ (**IIc**; Sebbar *et al.*, 2014) and C_5H_8NO2 (**IId**; Sebbar *et al.*, 2016) (Fig. 12) are matching candidates. Other examples with *R*1 = 4-FC_6H_4 and *R*2 = $CH_2C{\equiv}CH$ (Hni *et al.*, 2019) and *R*1 = 2-ClC_6H_4, *R*2 = $CH_2C{\equiv}CH$ (Sebbar *et al.*, 2017) are also known.

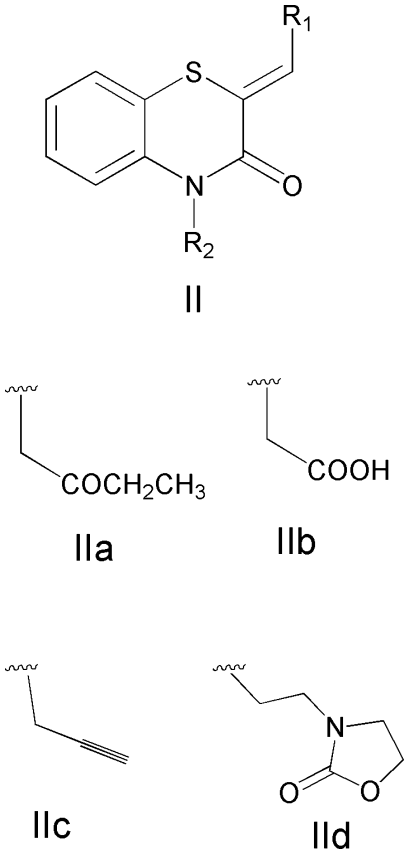

Figure 12
The molecular moieties (II) used for the CSD database search.

Table 4
Experimental details.

Crystal data	
Chemical formula	$C_8H_7NO_3S$
M_r	197.21
Crystal system, space group	Monoclinic, $P2_1/n$
Temperature (K)	125
a, *b*, *c* (Å)	7.2179 (6), 9.5043 (8), 11.9945 (9)
β (°)	97.584 (2)
V (Å^3)	815.64 (11)
Z	4
Radiation type	Mo $K\alpha$
μ (mm^{-1})	0.37
Crystal size (mm)	0.39 × 0.21 × 0.16
Data collection	
Diffractometer	Bruker D8 QUEST PHOTON 3 diffractometer
Absorption correction	Multi-scan (*SADABS*; Krause *et al.*, 2015)
T_{min}, T_{max}	0.91, 0.94
No. of measured, independent and observed [$I > 2\sigma(I)$] reflections	47688, 3957, 3739
R_{int}	0.027
(sin $\theta/\lambda)_{max}$ (Å^{-1})	0.836
Refinement	
$R[F^2 > 2\sigma(F^2)]$, $wR(F^2)$, *S*	0.025, 0.074, 1.04
No. of reflections	3957
No. of parameters	122
No. of restraints	1
H-atom treatment	H atoms treated by a mixture of independent and constrained refinement
$\Delta\rho_{max}$, $\Delta\rho_{min}$ (e Å^{-3})	0.52, −0.36

Computer programs: *APEX4* and *SAINT* (Bruker, 2021), *SHELXT* (Sheldrick, 2015*a*), *SHELXL2018/1* (Sheldrick, 2015*b*), *DIAMOND* (Brandenburg & Putz, 2012) and *SHELXTL* (Sheldrick, 2008).

8. Synthesis and crystallization

3,4-Dihydro-2*H*-1,4-benzothiazin-3-one (1.2 mmol) was dissolved in 3 ml of acetic acid and added dropwise into a solution of potassium permanganate (1.81 mmol) in 6 ml of water. After stirring for one h at room temperature, a solution of sodium thiosulfate pentahydrate (20%$_{wt}$) was added to react with excessive potassium permanganate. The precipitate obtained was filtered and recrystallized from ethanol to yield single-crystals suitable for X-ray structure analysis..

9. Refinement

Crystal data, data collection and structure refinement details are summarized in Table 4. H-atoms attached to carbon were placed in calculated positions (C—H = 0.95–0.99 Å) and were included as riding contributions with isotropic displacement parameters 1.2 or 1.5 times those of the attached atoms. That attached to nitrogen was placed in a location derived from a difference map and refined with a DFIX 0.91 0.01 instruction.

Two reflections affected by the beamstop were omitted from the final refinement.

Funding information

JTM thanks Tulane University for support of the Tulane Crystallography Laboratory. TH is grateful to Hacettepe University Scientific Research Project Unit (grant No. 013 D04 602 004).

References

Abbas, E. M. & Farghaly, T. A. (2010). *Monatsh. Chem.* **141**, 661–667.

Bakavoli, M., Sadeghian, H., Tabatabaei, Z., Rezaei, E., Rahimizadeh, M. & Nikpour, M. (2008). *J. Mol. Model.* **14**, 471–478.

Becke, A. D. (1993). *J. Chem. Phys.* **98**, 5648–5652.

Brandenburg, K. & Putz, H. (2012). *DIAMOND*. Crystal Impact GbR, Bonn, Germany.

Bruker (2021). *APEX4* and *SAINT*. Bruker AXS LLC, Madison, Wisconsin, USA.

Corelli, F., Manetti, F., Tafi, A., Campiani, G., Nacci, V. & Botta, M. (1997). *J. Med. Chem.* **40**, 125–131.

Cremer, D. & Pople, J. A. (1975). *J. Am. Chem. Soc.* **97**, 1354–1358.

Fringuelli, R., Milanese, L. & Schiaffella, F. (2005). *Mini Rev. Med. Chem.* **5**, 1061–1073.

Frisch, M. J., Trucks, G. W., Schlegel, H. B., Scuseria, G. E., Robb, M. A., Cheeseman, J. R., Scalmani, G., Barone, V., Mennucci, B., Petersson, G. A., Nakatsuji, H., Caricato, M., Li, X., Hratchian, H. P., Izmaylov, A. F., Bloino, J., Zheng, G., Sonnenberg, J. L., Hada, M., Ehara, M., Toyota, K., Fukuda, R., Hasegawa, J., Ishida, M., Nakajima, T., Honda, Y., Kitao, O., Nakai, H., Vreven, T., Montgomery, J. A. Jr, Peralta, J. E., Ogliaro, F., Bearpark, M., Heyd, J. J., Brothers, E., Kudin, K. N., Staroverov, V. N., Kobayashi, R., Normand, J., Raghavachari, K., Rendell, A., Burant, J. C., Iyengar, S. S., Tomasi, J., Cossi, M., Rega, N., Millam, J. M., Klene, M., Knox, J. E., Cross, J. B., Bakken, V., Adamo, C., Jaramillo, J., Gomperts, R., Stratmann, R. E., Yazyev, O., Austin, A. J., Cammi, R., Pomelli, C., Ochterski, J. W., Martin, R. L., Morokuma, K., Zakrzewski, V. G., Voth, G. A., Salvador, P., Dannenberg, J. J., Dapprich, S., Daniels, A. D., Farkas, O., Foresman, J. B., Ortiz, J. V., Cioslowski, J. & Fox, D. J. (2009). *GAUSSIAN09*. Gaussian Inc., Wallingford, CT, US

Gowda, J., Khader, A. M. A., Kalluraya, B., Shree, P. & Shabaraya, A. R. (2011). *Eur. J. Med. Chem.* **46**, 4100–4106.

Groom, C. R., Bruno, I. J., Lightfoot, M. P. & Ward, S. C. (2016). *Acta Cryst.* B**72**, 171–179.

Hathwar, V. R., Sist, M., Jørgensen, M. R. V., Mamakhel, A. H., Wang, X., Hoffmann, C. M., Sugimoto, K., Overgaard, J. & Iversen, B. B. (2015). *IUCrJ*, **2**, 563–574.

Hirshfeld, H. L. (1977). *Theor. Chim. Acta*, **44**, 129–138.

Hni, B., Sebbar, N. K., Hökelek, T., Ouzidan, Y., Moussaif, A., Mague, J. T. & Essassi, E. M. (2019). *Acta Cryst.* E**75**, 372–377.

Jayatilaka, D., Grimwood, D. J., Lee, A., Lemay, A., Russel, A. J., Taylor, C., Wolff, S. K., Cassam-Chenai, P. & Whitton, A. (2005). *TONTO* - A System for Computational Chemistry. Available at: http://hirshfeldsurface.net/

Kamila, S., Koh, B., Zhang, H. & Biehl, E. R. (2006). *Arkivoc*, **2**, 1–14.

Krause, L., Herbst-Irmer, R., Sheldrick, G. M. & Stalke, D. (2015). *J. Appl. Cryst.* **48**, 3–10.

Mackenzie, C. F., Spackman, P. R., Jayatilaka, D. & Spackman, M. A. (2017). *IUCrJ*, **4**, 575–587.

McKinnon, J. J., Jayatilaka, D. & Spackman, M. A. (2007). *Chem. Commun.* 3814–3816.

Sebbar, G., Mohamed, E., Hökelek, T., Mague, J. T., Sebbar, N. K., Essassi, E. M. & Belkadi, B. (2020*a*). *Acta Cryst.* E**76**, 629–636.

Sebbar, N. K., Ellouz, M., Ouzidan, Y., Kaur, M., Essassi, E. M. & Jasinski, J. P. (2017). *IUCrData*, **2**, x170889.

Sebbar, N. K., Labd, T. M., Ellouz, M., Essassi, E. M., Zerzouf, A., Karrouchi, K., Ouzidan, Y., Mennane, Z. & Mague, J. T. (2020*b*). *Iran. J. Chem. Chem. Eng.* **39**, 53–67.

Sebbar, N. K., Mekhzoum, M. E. M., Essassi, E. M., Zerzouf, A., Talbaoui, A., Bakri, Y., Saadi, M. & Ammari, L. E. (2016). *Res. Chem. Intermed.* **42**, 6845–6862.

Sebbar, N. K., Zerzouf, A., Essassi, E. M., Saadi, M. & El Ammari, L. (2014). *Acta Cryst.* E**70**, o614.

Sheldrick, G. M. (2008). *Acta Cryst.* A**64**, 112–122.

Sheldrick, G. M. (2015*a*). *Acta Cryst.* A**71**, 3–8.

Sheldrick, G. M. (2015*b*). *Acta Cryst.* C**71**, 3–8.

Spackman, M. A., McKinnon, J. J. & Jayatilaka, D. (2008). *CrystEngComm*, **10**, 377–388.

Spackman, P. R., Turner, M. J., McKinnon, J. J., Wolff, S. K., Grimwood, D. J., Jayatilaka, D. & Spackman, M. A. (2021). *J. Appl. Cryst.* **54**, 1006–1011.

Turner, M. J., Grabowsky, S., Jayatilaka, D. & Spackman, M. A. (2014). *J. Phys. Chem. Lett.* **5**, 4249–4255.

Turner, M. J., McKinnon, J. J., Jayatilaka, D. & Spackman, M. A. (2011). *CrystEngComm*, **13**, 1804–1813.

Turner, M. J., Thomas, S. P., Shi, M. W., Jayatilaka, D. & Spackman, M. A. (2015). *Chem. Commun.* **51**, 3735–3738.

Venkatesan, P., Thamotharan, S., Ilangovan, A., Liang, H. & Sundius, T. (2016). *Spectrochim. Acta A Mol. Biomol. Spectrosc.* **153**, 625–636.

Warren, B. K. & Knaus, E. E. (1987). *Eur. J. Med. Chem.* **22**, 411–415.

supporting information

Acta Cryst. (2023). E**79**, 1037-1043 [https://doi.org/10.1107/S205698902300868X]

Crystal structure, Hirshfeld surface and crystal void analysis, intermolecular interaction energies, DFT calculations and energy frameworks of 2*H*-benzo[*b*][1,4]thiazin-3(4*H*)-one 1,1-dioxide

Ezaddine Irrou, Younesse Ait Elmachkouri, Ahmed Mazzah, Tuncer Hökelek, Amal Haoudi, Joel T. Mague, Mohamed Labd Taha and Nada Kheira Sebbar

Computing details

Data collection: *APEX4* (Bruker, 2021); cell refinement: *SAINT* (Bruker, 2021); data reduction: *SAINT* (Bruker, 2021); program(s) used to solve structure: *SHELXT* (Sheldrick, 2015*a*); program(s) used to refine structure: *SHELXL2018/1* (Sheldrick, 2015*b*); molecular graphics: *DIAMOND* (Brandenburg & Putz, 2012); software used to prepare material for publication: *SHELXTL* (Sheldrick, 2008).

2*H*-Benzo[*b*][1,4]thiazin-3(4*H*)-one 1,1-dioxide

Crystal data

$C_8H_7NO_3S$
M_r = 197.21
Monoclinic, $P2_1/n$
a = 7.2179 (6) Å
b = 9.5043 (8) Å
c = 11.9945 (9) Å
β = 97.584 (2)°
V = 815.64 (11) Å^3
Z = 4
$F(000)$ = 408
D_x = 1.606 Mg m^{-3}
Mo $K\alpha$ radiation, λ = 0.71073 Å
Cell parameters from 9215 reflections
θ = 2.9–36.4°
μ = 0.37 mm^{-1}
T = 125 K
Prism, colourless
0.39 × 0.21 × 0.16 mm

Data collection

Bruker D8 QUEST PHOTON 3 diffractometer
Radiation source: fine-focus sealed tube
Graphite monochromator
Detector resolution: 7.3910 pixels mm^{-1}
φ and ω scans
Absorption correction: multi-scan (*SADABS*; Krause *et al.*, 2015)
T_{min} = 0.91, T_{max} = 0.94
47688 measured reflections
3957 independent reflections
3739 reflections with $I > 2\sigma(I)$
R_{int} = 0.027
θ_{max} = 36.4°, θ_{min} = 3.6°
h = −12→12
k = −15→15
l = −19→20

Refinement

Refinement on F^2
Least-squares matrix: full
$R[F^2 > 2\sigma(F^2)]$ = 0.025
$wR(F^2)$ = 0.074
S = 1.04
3957 reflections
122 parameters
1 restraint
Primary atom site location: dual

Secondary atom site location: difference Fourier map	$w = 1/[\sigma^2(F_o^2) + (0.0383P)^2 + 0.2724P]$ where $P = (F_o^2 + 2F_c^2)/3$
Hydrogen site location: mixed	$(\Delta/\sigma)_{max} = 0.001$
H atoms treated by a mixture of independent and constrained refinement	$\Delta\rho_{max} = 0.52$ e Å^{-3}
	$\Delta\rho_{min} = -0.36$ e Å^{-3}

Special details

Experimental. The diffraction data were obtained from 9 sets of frames, each of width 0.5° in ω or φ, collected with scan parameters determined by the "strategy" routine in *APEX4*. The scan time was 15 sec/frame.

Geometry. All esds (except the esd in the dihedral angle between two l.s. planes) are estimated using the full covariance matrix. The cell esds are taken into account individually in the estimation of esds in distances, angles and torsion angles; correlations between esds in cell parameters are only used when they are defined by crystal symmetry. An approximate (isotropic) treatment of cell esds is used for estimating esds involving l.s. planes.

Refinement. Refinement of F^2 against ALL reflections. The weighted R-factor wR and goodness of fit S are based on F^2, conventional R-factors R are based on F, with F set to zero for negative F^2. The threshold expression of $F^2 > 2\text{sigma}(F^2)$ is used only for calculating R-factors(gt) etc. and is not relevant to the choice of reflections for refinement. R-factors based on F^2 are statistically about twice as large as those based on F, and R- factors based on ALL data will be even larger.

Fractional atomic coordinates and isotropic or equivalent isotropic displacement parameters (Å²)

	x	*y*	*z*	U_{iso}*/U_{eq}
S1	0.16068 (2)	0.52143 (2)	0.71754 (2)	0.01099 (4)
O1	0.61228 (8)	0.59530 (6)	0.90859 (5)	0.01991 (10)
O2	0.16268 (8)	0.66721 (6)	0.68352 (5)	0.01797 (10)
O3	−0.01882 (7)	0.45794 (7)	0.72667 (5)	0.01832 (10)
N1	0.57806 (8)	0.47975 (6)	0.74211 (5)	0.01411 (10)
H1	0.7001 (12)	0.4900 (15)	0.7398 (13)	0.027 (3)*
C1	0.27959 (8)	0.42044 (6)	0.62800 (5)	0.01059 (9)
C2	0.17997 (9)	0.35615 (7)	0.53412 (5)	0.01342 (10)
H2	0.047397	0.361237	0.521776	0.016*
C3	0.27651 (11)	0.28460 (7)	0.45882 (6)	0.01663 (11)
H3	0.210847	0.242727	0.393292	0.020*
C4	0.47092 (11)	0.27481 (8)	0.48036 (6)	0.01841 (12)
H4	0.536825	0.224837	0.429380	0.022*
C5	0.56985 (10)	0.33681 (8)	0.57499 (6)	0.01630 (11)
H5	0.701938	0.327605	0.588942	0.020*
C6	0.47486 (8)	0.41274 (7)	0.64966 (5)	0.01164 (10)
C7	0.51172 (9)	0.53288 (7)	0.83499 (5)	0.01315 (10)
C8	0.30863 (9)	0.50214 (7)	0.84603 (5)	0.01299 (10)
H8A	0.266578	0.566751	0.902374	0.016*
H8B	0.298167	0.404753	0.873825	0.016*

Atomic displacement parameters (Å²)

	U^{11}	U^{22}	U^{33}	U^{12}	U^{13}	U^{23}
S1	0.00776 (7)	0.01295 (7)	0.01219 (7)	0.00109 (4)	0.00109 (4)	−0.00153 (4)
O1	0.0173 (2)	0.0236 (3)	0.0174 (2)	−0.00682 (19)	−0.00298 (17)	−0.00209 (18)
O2	0.0205 (2)	0.0129 (2)	0.0200 (2)	0.00460 (17)	0.00061 (18)	0.00015 (16)
O3	0.00783 (18)	0.0262 (3)	0.0214 (2)	−0.00199 (17)	0.00373 (16)	−0.00439 (19)

N1	0.0078 (2)	0.0195 (2)	0.0149 (2)	−0.00112 (17)	0.00092 (16)	0.00008 (18)
C1	0.0092 (2)	0.0114 (2)	0.0113 (2)	0.00061 (16)	0.00190 (16)	−0.00003 (16)
C2	0.0138 (2)	0.0137 (2)	0.0125 (2)	−0.00096 (19)	0.00073 (18)	−0.00101 (18)
C3	0.0212 (3)	0.0150 (3)	0.0140 (2)	−0.0010 (2)	0.0038 (2)	−0.00282 (19)
C4	0.0218 (3)	0.0166 (3)	0.0184 (3)	0.0025 (2)	0.0088 (2)	−0.0024 (2)
C5	0.0133 (2)	0.0177 (3)	0.0190 (3)	0.0033 (2)	0.0064 (2)	0.0004 (2)
C6	0.0093 (2)	0.0130 (2)	0.0130 (2)	0.00103 (17)	0.00242 (17)	0.00133 (17)
C7	0.0114 (2)	0.0143 (2)	0.0133 (2)	−0.00146 (18)	−0.00035 (18)	0.00154 (18)
C8	0.0115 (2)	0.0162 (2)	0.0113 (2)	−0.00114 (19)	0.00154 (18)	−0.00122 (18)

Geometric parameters (Å, º)

S1—O2	1.4450 (6)	C2—H2	0.9500
S1—O3	1.4464 (6)	C3—C4	1.3960 (11)
S1—C1	1.7478 (6)	C3—H3	0.9500
S1—C8	1.7649 (7)	C4—C5	1.3898 (11)
O1—C7	1.2203 (8)	C4—H4	0.9500
N1—C7	1.3661 (9)	C5—C6	1.3982 (9)
N1—C6	1.4043 (9)	C5—H5	0.9500
N1—H1	0.890 (8)	C7—C8	1.5175 (9)
C1—C2	1.3945 (9)	C8—H8A	0.9900
C1—C6	1.4010 (9)	C8—H8B	0.9900
C2—C3	1.3892 (10)		
O2—S1—O3	117.64 (4)	C5—C4—C3	121.22 (6)
O2—S1—C1	109.21 (3)	C5—C4—H4	119.4
O3—S1—C1	109.56 (3)	C3—C4—H4	119.4
O2—S1—C8	108.59 (3)	C4—C5—C6	119.96 (6)
O3—S1—C8	109.59 (3)	C4—C5—H5	120.0
C1—S1—C8	100.95 (3)	C6—C5—H5	120.0
C7—N1—C6	127.24 (6)	C5—C6—C1	118.33 (6)
C7—N1—H1	116.1 (10)	C5—C6—N1	119.08 (6)
C6—N1—H1	116.7 (10)	C1—C6—N1	122.58 (6)
C2—C1—C6	121.72 (6)	O1—C7—N1	122.05 (6)
C2—C1—S1	119.61 (5)	O1—C7—C8	121.31 (6)
C6—C1—S1	118.58 (5)	N1—C7—C8	116.53 (6)
C3—C2—C1	119.34 (6)	C7—C8—S1	112.57 (4)
C3—C2—H2	120.3	C7—C8—H8A	109.1
C1—C2—H2	120.3	S1—C8—H8A	109.1
C2—C3—C4	119.38 (6)	C7—C8—H8B	109.1
C2—C3—H3	120.3	S1—C8—H8B	109.1
C4—C3—H3	120.3	H8A—C8—H8B	107.8
O2—S1—C1—C2	−93.69 (6)	C2—C1—C6—C5	−0.74 (9)
O3—S1—C1—C2	36.48 (6)	S1—C1—C6—C5	−177.28 (5)
C8—S1—C1—C2	152.03 (5)	C2—C1—C6—N1	178.32 (6)
O2—S1—C1—C6	82.92 (6)	S1—C1—C6—N1	1.78 (8)
O3—S1—C1—C6	−146.91 (5)	C7—N1—C6—C5	−165.40 (7)

C8—S1—C1—C6	−31.36 (6)	C7—N1—C6—C1	15.55 (10)
C6—C1—C2—C3	−1.16 (10)	C6—N1—C7—O1	−176.50 (7)
S1—C1—C2—C3	175.34 (5)	C6—N1—C7—C8	7.37 (10)
C1—C2—C3—C4	1.92 (10)	O1—C7—C8—S1	141.26 (6)
C2—C3—C4—C5	−0.81 (11)	N1—C7—C8—S1	−42.58 (7)
C3—C4—C5—C6	−1.12 (11)	O2—S1—C8—C7	−64.45 (5)
C4—C5—C6—C1	1.86 (10)	O3—S1—C8—C7	165.81 (5)
C4—C5—C6—N1	−177.23 (6)	C1—S1—C8—C7	50.29 (5)

Hydrogen-bond geometry (Å, º)

*Cg*2 is the centroid of the C1–C6 benzene ring.

D—H···*A*	*D*—H	H···*A*	*D*···*A*	*D*—H···*A*
N1—H1···O3^{i}	0.89 (1)	2.08 (1)	2.9472 (8)	165 (1)
C5—H5···O1^{ii}	0.95	2.58	3.2330 (9)	126
C8—H8*A*···*Cg*2^{iii}	0.99	2.93	3.7933 (8)	146
C8—H8*B*···O2^{iv}	0.99	2.39	3.2126 (9)	140

Symmetry codes: (i) *x*+1, *y*, *z*; (ii) −*x*+3/2, *y*−1/2, −*z*+3/2; (iii) −*x*+1/2, *y*+1/2, −*z*+3/2; (iv) −*x*+1/2, *y*−1/2, −*z*+3/2.